ORGANISATION EUROPEENNE POUR LA RECHERCHE NUCLEAIRE
EUROPEAN ORGANIZATION FOR NUCLEAR RESEARCH
Laboratoire Européen pour la Physique des Particules
European Laboratory for Particle Physics

Occupational Health & Safety and Environmental Protection Unit

Summer Student Report
1 August 2025

Impact of Interaction Materials Shower Development in High-Energy Neutrino Interactions for Radiation Protection Calculations at Muon Collider

prepared by:	**verified by:**	**approved by:**
C. V. Valdivieso Castillo (SY-STI/HSE-RP)	J. Manczak (SY-STI / HSE-RP) C. Ahdida (HSE-RP)	J. Manczak (SY-STI / HSE-RP) C. Ahdida (HSE-RP)

Contents

1 Introduction

The Muon Collider will produce an intense flux of high-energy neutrinos (TeV scale), which, due to their extremely low interaction probability, can travel vast distances through the Earth and induce secondary particle showers at the Earth's surface. Although the neutrino cross section is small, the combination of their high energy and an enormous production rate ($\sim 10^9$ decays per meter per second) requires careful analysis to ensure compliance with radiation protection objectives, which are set to less than 10 $\mu Sv/year$ for the general public.

This research was divided into two main parts:

- **Neutrino Distributions:** Characterization of the energy and angular spectra of neutrinos produced by the decay of $5\,\mathrm{TeV}$ muons. In addition, total interaction cross sections were computed individually for each neutrino flavor (ν_μ, $\bar{\nu}_\mu$, ν_e, $\bar{\nu}_e$) and for each target material (soil, dry moraine, wet moraine, sea, water, concrete and iron) using FLUKA Monte Carlo simulations.
- **Neutrino Effective Dose:** Quantitative assessment of the radiological impact of these neutrinos when interacting with materials at the Earth's surface. For water, dry moraine, wet moraine and iron, the effective dose induced by neutrinos of each flavour was evaluated.

2 Neutrino Distributions

Each muon decay produces an electron or positron and two neutrinos of opposite flavor. While the electrons interact locally, neutrinos travel long distances through the ground and can reach the Earth's surface. Because of the high energy of the muons, the neutrinos are emitted in very narrow cones pointing forward. As the muons circulate in the collider ring, this leads to the formation of a thin disk of neutrino radiation. The straight sections of the ring produce even stronger neutrino beams, since many muons decay in the same direction.

To study how these neutrinos contribute to radiation exposure at the Earth's surface, a set of simulations was performed to characterize the energy and angular distributions of interacting neutrinos and antineutrinos resulting from $5\,\mathrm{TeV}$ muon decays. The analysis was carried out separately for different materials: soil, water, concrete, iron, dry moraine and wet moraine, and for each neutrino flavor: ν_e, $\bar{\nu}_e$, ν_μ and $\bar{\nu}_\mu$.

The interacting neutrino distributions shown in Figure 2 and 1 were obtained using neutrino-nucleon cross sections extracted from FLUKA. These values correspond to interactions with free protons and neutrons and are evaluated as a function of neutrino energy. While this method allows for efficient estimation of interaction rates, it does not account for nuclear effects such as Fermi motion and Pauli blocking, which would require dedicated simulations for each neutrino energy. As a result of this simplified treatment, the spectral distributions are expected to remain essentially identical across different target materials, as observed in the figures below.

The interacting neutrino distributions shown in Figure 1 and 2, were obtained by applying a simplified cross section model to the output of FLUKA simulations. Specifically, macroscopic cross sections $\Sigma(E)$ were calculated for each neutrino flavor and target material using the expression $\Sigma(E) = N_p \cdot \sigma_p(E) + N_n \cdot \sigma_n(E)$, where N_p and N_n are the number densities of protons and neutrons, respectively, and σ_p, σ_n are the microscopic cross sections provided by FLUKA. This approach provides a consistent normalization factor across materials while preserving the spectral shape driven by the neutrino flavor. As a result, the spectral distributions are expected to remain essentially identical across different target materials, as observed in the figures below.

Figure 1 shows the energy spectra of interacting neutrinos in various materials, revealing that muon-flavored neutrinos tend to have higher average energies compared to the electron-flavored ones. This observation is further confirmed in Figure 2, where the spectra for each flavor are shown individually and compared across the interaction materials. Notably, the energy distributions remain virtually unchanged across materials, indicating that the spectral shape is governed by neutrino flavor rather than by the interaction medium.

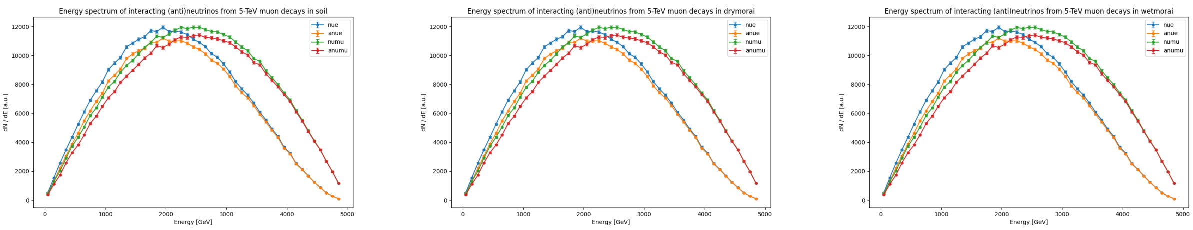

a) b) c)

Figure 1: Energy Spectrum of interacting neutrinos and antineutrinos from 5 TeV μ decays in different materials: a) soil, b) dry moray and c) wet moray.

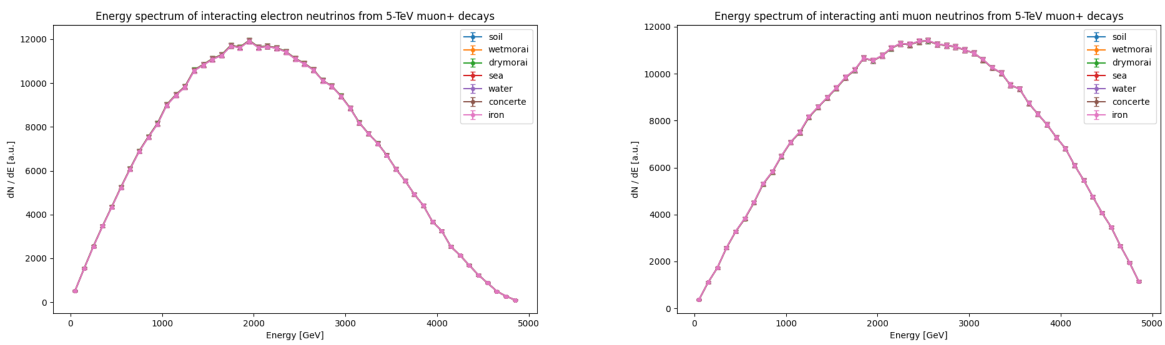

a) b)

Figure 2: Energy Spectrum of interacting: a) electron neutrinos ν_e and b) anti muon neutrinos $\bar{\nu}_\mu$, from 5 TeV μ^+ decays in different materials

Angular distributions were also evaluated, as shown in Figures 3 and 4. The results confirm that the neutrino flux is strongly forward-peaked, forming a narrow cone aligned with the parent muon trajectory. Higher-energy neutrinos are more tightly collimated, staying close to the beam axis, while lower-energy ones are emitted at wider angles. This behavior implies a dose distribution that is both energy- and direction-dependent, with most of the radiological impact concentrated near the central axis of emission.

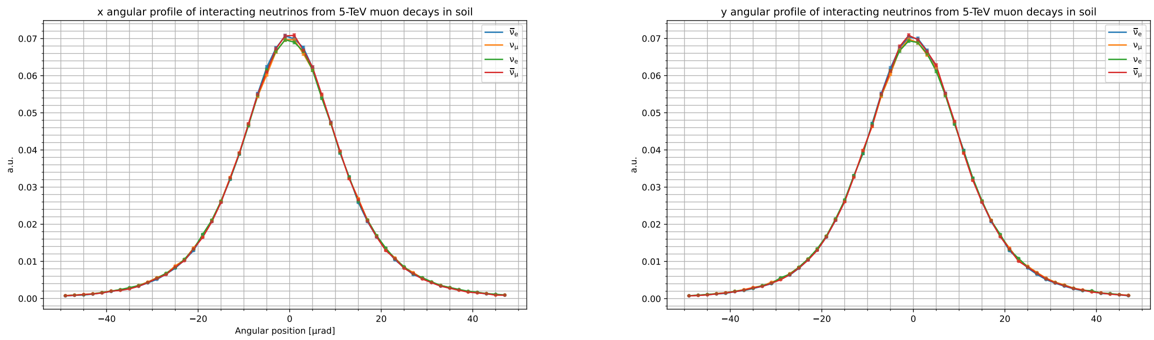

a) b)

Figure 3: Angular profile of interacting neutrinos from 5 TeV μ decays in soil: a) X axis profile and b) Y axis profile.

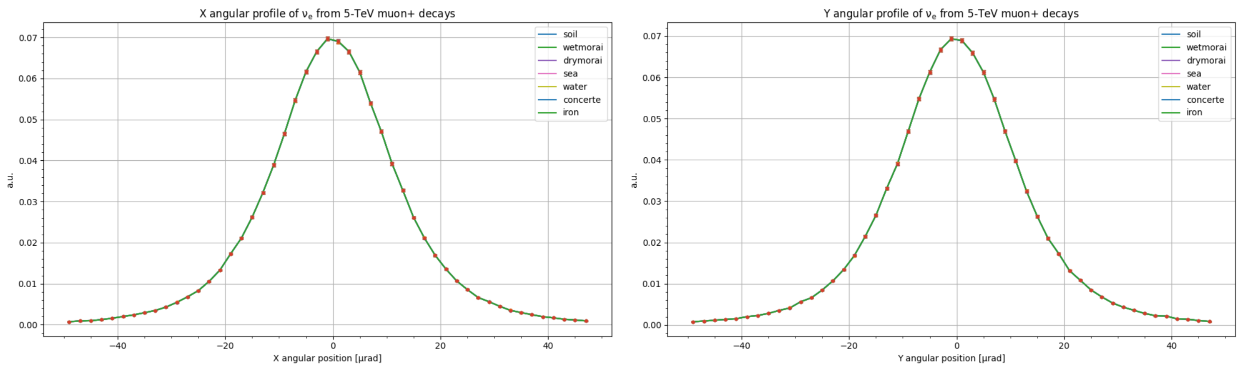

a) b)

Figure 4: Angular profile of interacting neutrinos from 5 TeV μ decays in different materials: a) X axis profile and b) Y axis profile.

Lastly, the computed macroscopic cross sections for each neutrino flavor and material are summarized in Table 1. These values, derived from the simplified model introduced earlier, reflect the combined effect of material density and composition on the interaction probability. While the energy and angular spectra remain largely unaffected by the choice of material, being primarily determined by neutrino flavor, the cross sections directly influence the overall normalization of the effective dose. In general, neutrinos exhibit larger cross sections than their antineutrino counterparts across all materials. As shown in Figures 5 and 6, these variations correlate with the density and elemental makeup of the target, affecting the total magnitude of radiation exposure, though not its spectral shape.

Additional plots showing the full set of energy and angular distributions for each neutrino flavor and material, including those not shown in the main text, are provided in the Appendix A for reference. These figures complement the analysis presented in this section and offer a more detailed view of the simulation results.

Material	Cross sec. ν_e	Cross sec. ν_μ	Cross sec. $\bar{\nu}_e$	Cross sec. $\bar{\nu}_\mu$
Soil	1.4017×10^{-11}	1.5801×10^{-11}	8.0227×10^{-12}	9.1059×10^{-12}
Water	6.8302×10^{-12}	7.7046×10^{-12}	4.0754×10^{-12}	4.6272×10^{-12}
Dry Morai	1.4059×10^{-11}	1.5834×10^{-11}	8.0161×10^{-12}	9.0901×10^{-12}
Wet Morai	1.4029×10^{-11}	1.5801×10^{-11}	8.0266×10^{-12}	9.1019×10^{-12}
Iron	5.6103×10^{-11}	6.3264×10^{-11}	3.1252×10^{-11}	3.5493×10^{-11}

Table 1: Macroscopic cross sections Σ for each neutrino flavor and material, as computed with FLUKA.

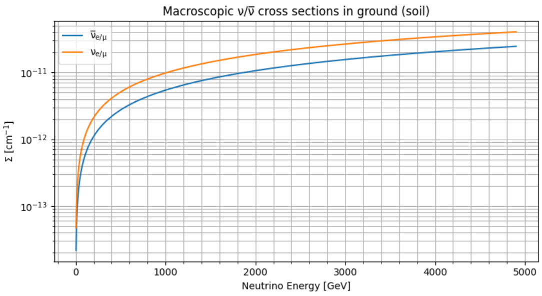

a)

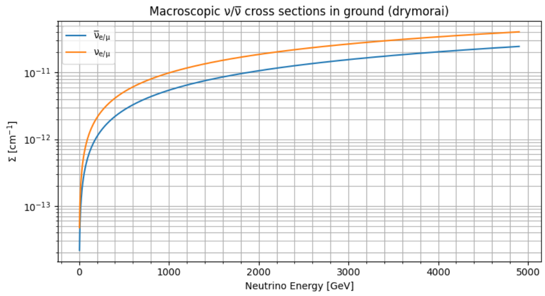

b)

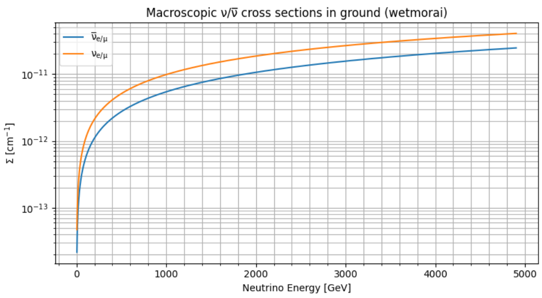

c)

Figure 5: Macroscopic ν_e, ν_μ, $\bar{\nu}_e$ and $\bar{\nu}_\mu$ cross sections in: a) soil, b) dry morai and c) wet morai.

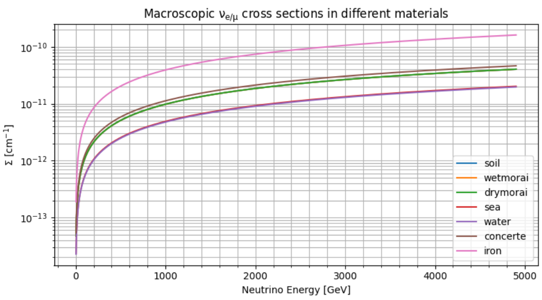

a)

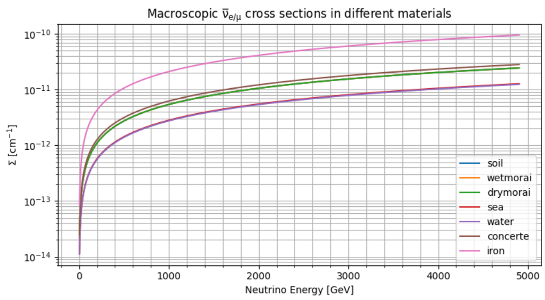

b)

Figure 6: Macroscopic cross sections in different materials: a) ν_e/ ν_μ, b) $\bar{\nu}_e/\bar{\nu}_\mu$

3 Effective Dose Distributions

The effective dose is a radiological quantity designed to estimate the total biological impact of ionizing radiation on the human body. Unlike the absorbed dose, which only quantifies the energy deposited per unit mass ($D = \Delta E/\Delta m$), the effective dose incorporates both the type of radiation and the varying sensitivity of different tissues and organs. This is achieved through the use of radiation weighting factors (w_R) and tissue weighting factors (w_T), as defined by the ICRP. The resulting equation is:

$$H = \sum_T w_T \cdot H_T = \sum_T w_T \cdot \sum_R w_R \cdot D_{T,R}$$

In the context of a high-energy muon collider, the effective dose quantifies the biological impact of secondary particle showers produced when neutrinos interact with surrounding materials. Despite their low interaction probability, the high flux and energy of neutrinos at a muon collider make these contributions non-negligible at the Earth's surface. Therefore, evaluating the effective dose is essential for demonstrating compliance with public radiation safety limits and guiding mitigation strategies.

To evaluate realistic exposure scenarios, FLUKA simulations were performed using a simplified geometry representing an underground room partially surrounded by soil. In this configuration, neutrinos travel through a layer of dense material before reaching a room filled with air. The neutrino beam axis is placed 1 m below the surface and interactions occurring approximately 20 km from the muon decay point.

Different materials: soil, concrete, iron, water, sea water, dry moraine and wet moraine, were used to model the surroundings. These vary in density and composition, which directly influences the development of secondary particle showers and, consequently, the resulting effective dose.

Figure 7 shows the Z-profile of the effective dose both outside and inside the room. Panel (a) corresponds to the air-filled room, while panel (b) shows the distribution in the surrounding dense soil. The contrast between the two regions is evident: outside the room, the dense medium attenuates the dose more efficiently, resulting in a sharper, more confined profile.

The corresponding X-profile is shown in Figure 8, highlighting a broader lateral spread within the air-filled room.

To quantitatively assess the spatial distribution of the effective dose, one-dimensional profiles were extracted along both the X and Z directions for different materials and neutrino flavours, inside and outside the room.

Figures 9 and 10 compare the dose distributions for electron neutrinos and anti-muon neutrinos. Inside the room, the absence of dense shielding (air) allows wide-angle secondaries to reach the measurement region, producing broad lateral spreads.

Outside the room, we have narrower profiles and reducing the dose magnitude. The soil acts as a natural shield, particularly effective in the case of iron.

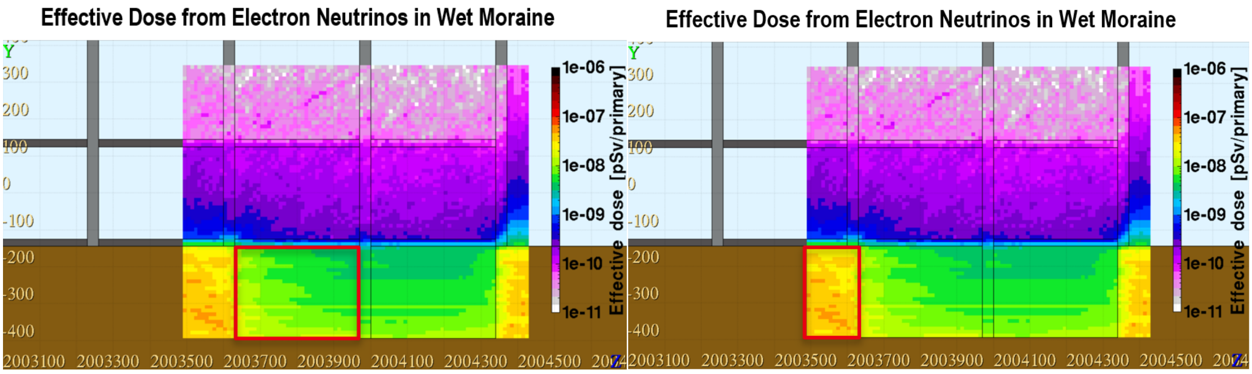

a) Inside the room

b) Outside the room

Figure 7: Z-profile of the effective dose from electron neutrinos interacting in wet moraine: a) inside the room (air), b) outside the room (soil).

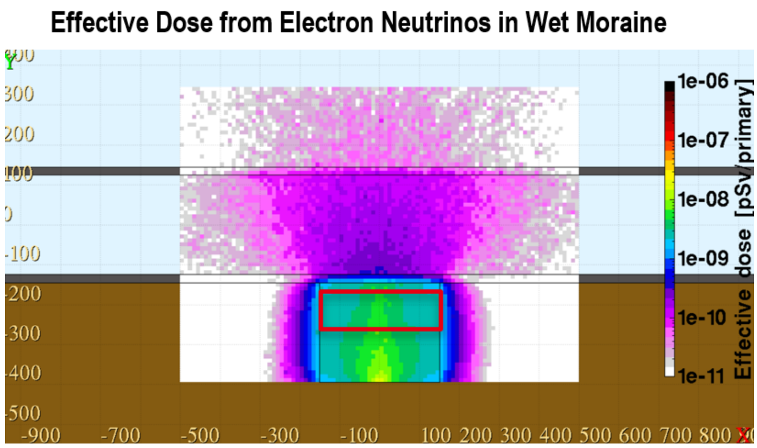

Figure 8: X-profile of the effective dose from electron neutrinos interacting in wet moraine.

Figure 11 presents the Z-profiles for both neutrino flavours. A clear dose drop is observed at the room entrance (marked by a red vertical line), indicating the transition from dense material to the air-filled volume. Inside the room, the dose profile flattens due to the lack of attenuation.

Taken together, these results confirm that the effective dose distribution is highly sensitive to the surrounding material composition—not only in magnitude but also in spatial shape. These findings highlight the importance of strategic material selection in the design of underground infrastructure for future muon collider facilities.

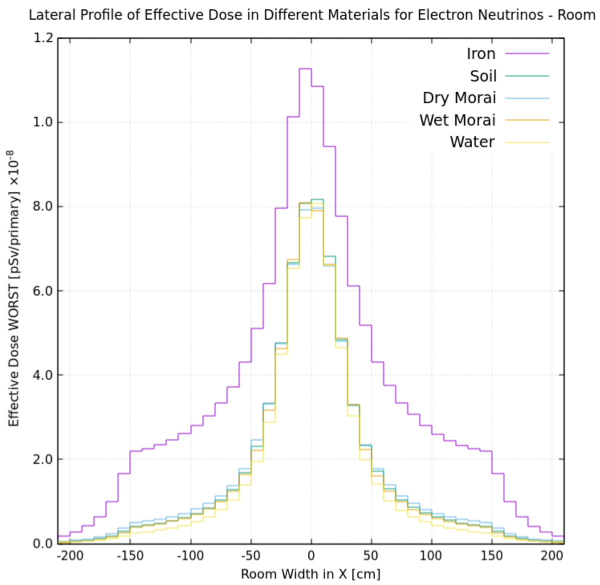

a) ν_e

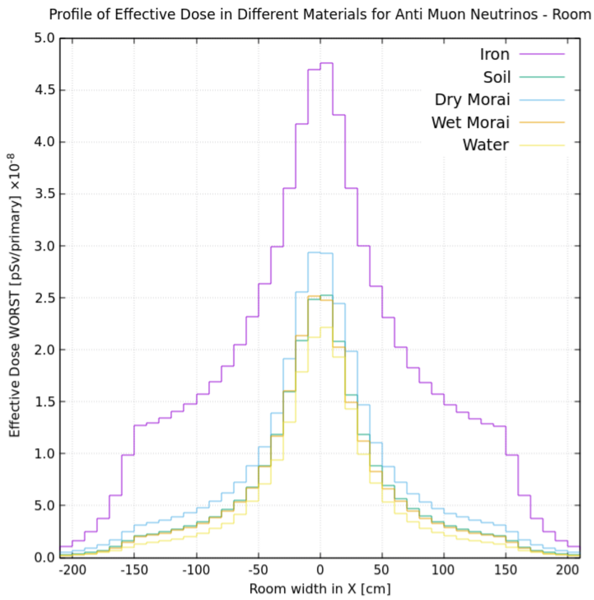

b) $\bar{\nu}_\mu$

Figure 9: Lateral (X) profiles of the effective dose **inside the room** for various materials: a) electron neutrinos, b) anti-muon neutrinos.

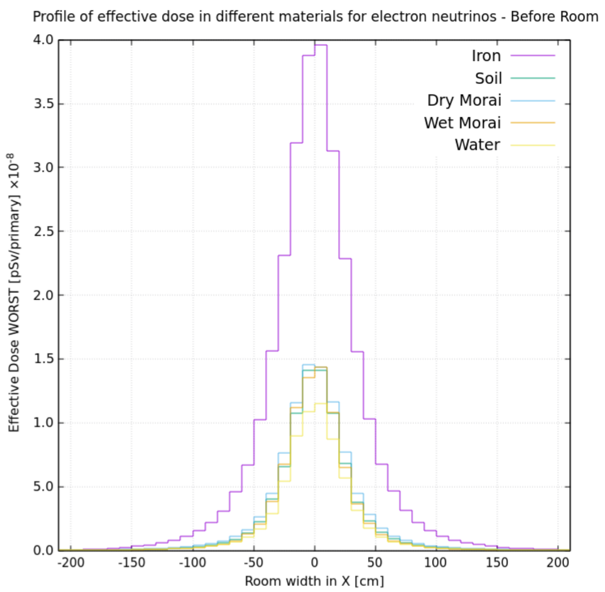

a) ν_e

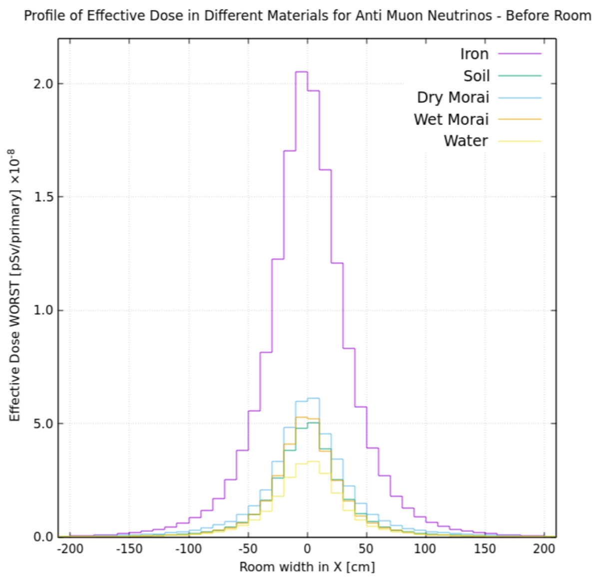

b) $\bar{\nu}_\mu$

Figure 10: Lateral (X) profiles of the effective dose **outside the room** for various materials: a) electron neutrinos, b) anti-muon neutrinos.

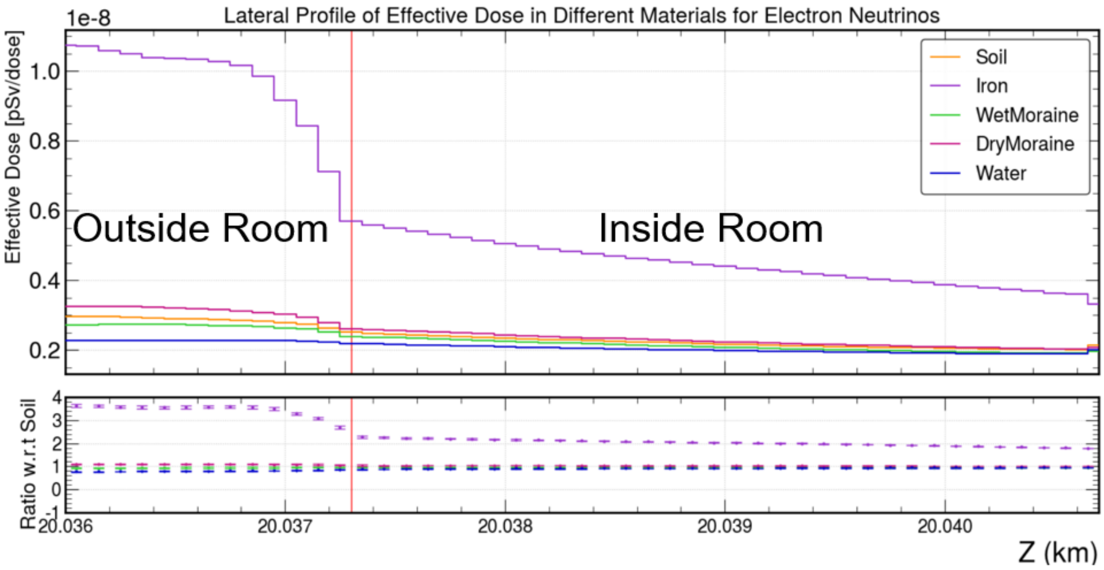

a) ν_e

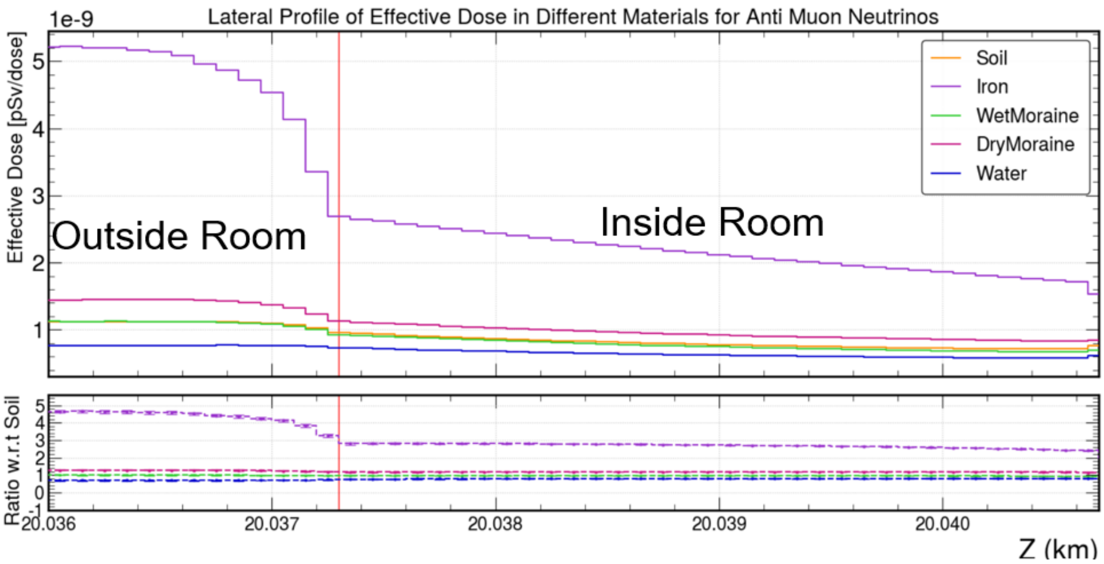

b) $\bar{\nu}_\mu$

Figure 11: Longitudinal (Z) profiles of the effective dose across the room boundary. Lower panels show the ratio with respect to soil. a) electron neutrinos, b) anti-muon neutrinos.

4 Conclusions

The evaluation of effective dose in the context of a high-energy muon collider highlights the importance of secondary particle showers produced by neutrino interactions with matter. These interactions, although rare, become non-negligible at TeV energies due to the large neutrino flux and their forward-focused angular distribution. The resulting showers are the primary contributors to effective dose, especially in underground or shielded environments.

Given the limited knowledge of the exact geological and structural composition at potential collider sites, simulations were carried out using a range of representative materials—such as soil, water, concrete, iron, and different moraine types. Each material exhibits unique density and elemental composition, which directly impacts the probability of interaction (via macroscopic cross sections) and the development of secondary showers. As shown, these variations affect the magnitude and spatial spread of the effective dose, particularly in confined spaces like rooms embedded in the terrain.

By comparing dose profiles across materials, we capture the systematic uncertainties that arise from environmental assumptions. This strategy not only improves the robustness of radiological risk assessments but also supports the design of shielding and safety protocols. Overall, the results provide a conservative and flexible framework for estimating neutrino-induced radiation, ensuring the safe implementation of future muon collider facilities.

It is worth noting that the neutrino interaction model used in this study assumes free nucleons and does not incorporate nuclear structure effects. While this simplification may slightly affect absolute normalization, it provides consistent spectral predictions across materials and remains appropriate for the objectives of this work.

Acknowledgments

We would like to show our gratitude to Claudia Ahdida and Jerzy Manczak for the excellent collaboration.

Appendices

A Appendix

:

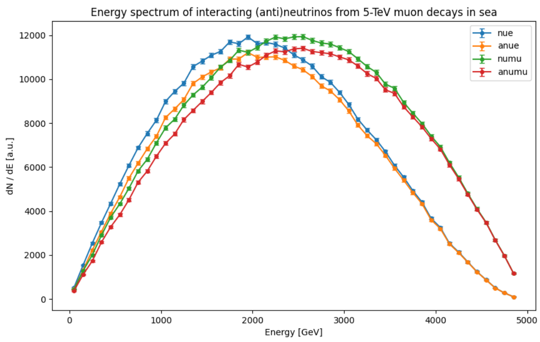

d)

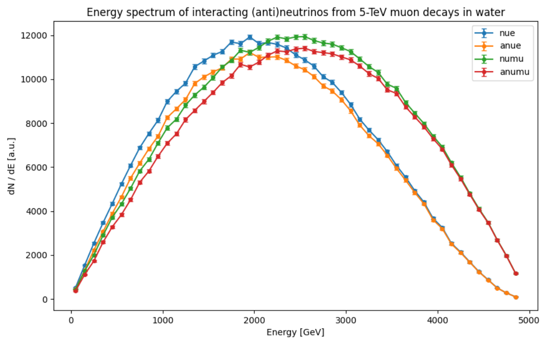

e)

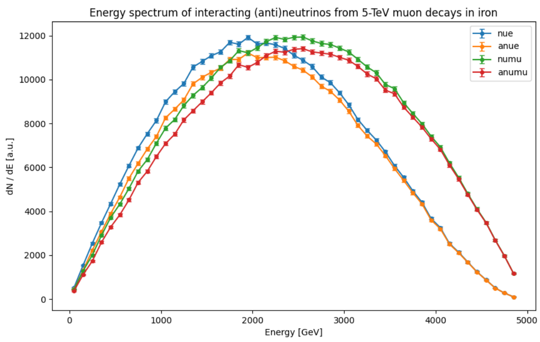

f)

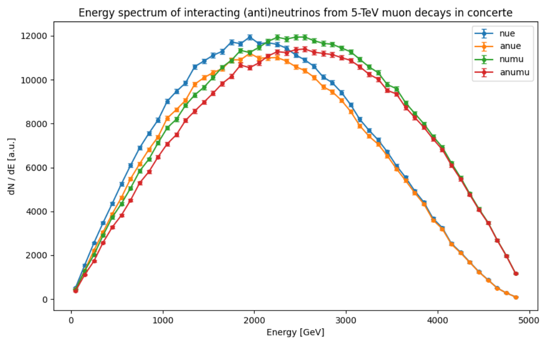

e)

Figure 12: Energy Spectrum of interacting neutrinos and antineutrinos from muon decays in different materials: d) sea, e) water, f) iron and g) concrete μ^+ decays.

B Appendix

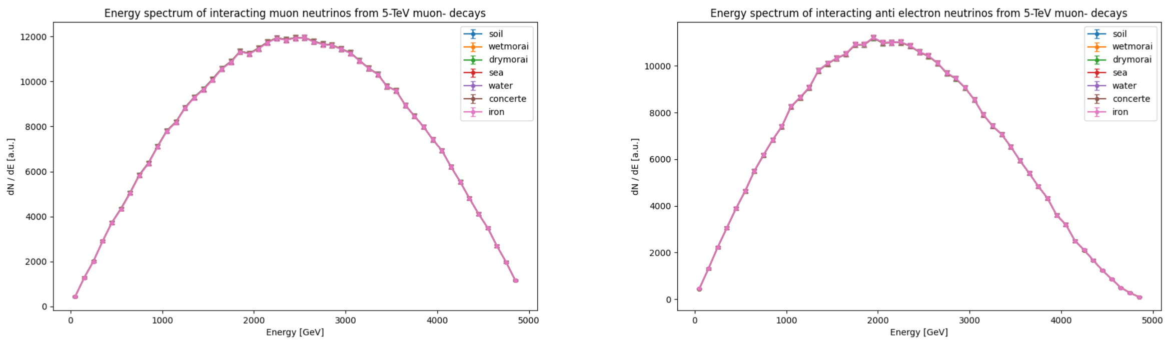

a) b)

Figure 13: Energy Spectrum of interacting: a) muon neutrinos ν_μ and b) anti electron neutrinos $\bar{\nu}_e$, from 5 TeV μ^- decays in different materials

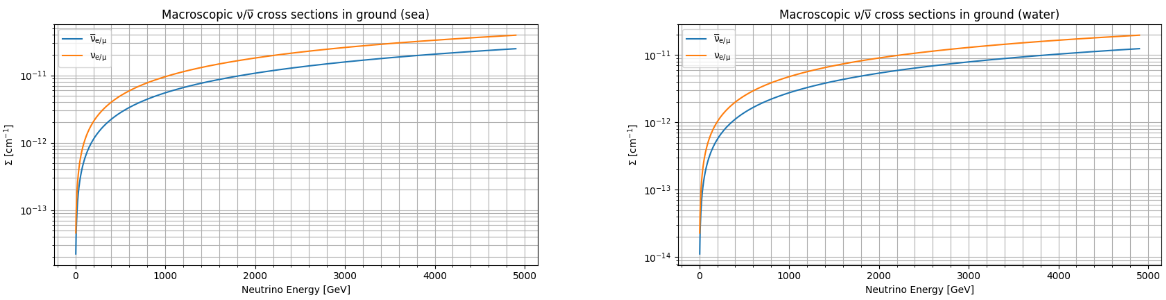

d) e)

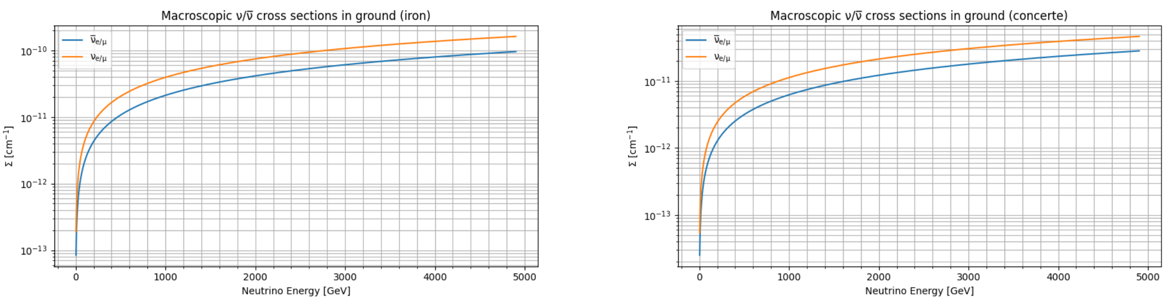

f) g)

Figure 14: Macroscopic ν_e, ν_μ, $\bar{\nu}_e$ and $\bar{\nu}_\mu$ cross sections in: d) sea, e) water, f) iron and g) concerte